Density Functional Theory and Atoms-in-Molecules Investigation of Intramolecular Hydrogen Bonding in Derivatives of Malonaldehyde and Implications for Resonance-Assisted Hydrogen Bonding

Jeffrey N. Woodford[†]

Department of Chemistry and Biochemistry, Eastern Oregon University, One University Boulevard, La Grande, Oregon 97850-2899

A density functional theory (DFT) and atoms-in-molecules (AIM) analysis has been applied to the intramolecular hydrogen bonding in the enol conformers of malonaldehyde and its fluoro-, chloro-, cyano-, and nitro-substituted derivatives. With the B3LYP/6-311++G(2d,p) method, good agreement between the DFT geometries and published experimental structures has been found. The donor−acceptor distance was also varied in a series of constrained optimizations in order to determine if energetic, structural, and topological trends associated with intermolecular hydrogen bonding remain valid in the intramolecular case. At very short donor−acceptor distances (<2.24 Å), the hydrogen is symmetrically located between donor and acceptor; at distances longer than this, the hydrogen bonding is no longer symmetric. The AIM methodology has been applied to explore the topology of the electron density in the intramolecular hydrogen bonds of the chosen model systems. Most AIM properties for intramolecular hydrogen bond distances longer than 2.24 Å show smooth trends, consistent with intermolecular hydrogen bonds. Integrated AIM properties have also been used to explore the phenomenon of resonance-assisted hydrogen bonding (RAHB). It is shown that as the donor−acceptor distance is varied, π-electron density is redistributed among the carbon atoms in the intramolecular hydrogen bond ring; however, contrary to prior studies, the integrated atomic charges on the donor−acceptor atoms were found to be insensitive to variation of hydrogen-bonding distance.

Introduction

The importance of the hydrogen bond cannot be overstated. Its chemical properties have both subtle and profound influences on the essential chemistry of life, crystal packing and engineering, self-assembly, solvation, catalysis, chelation, and a host of other important phenomena. Extensive research has been devoted to the nature of the hydrogen bond for nearly a century; only a few notable books and review articles on the subject may be cited here in this limited space.[1−9]

The Atoms in Molecules (AIM) theory[10] has become a powerful tool for understanding the properties of hydrogen bonds.[11−14] In the AIM theory, quantum-mechanical principles are applied to the electron density of a molecule in order to gain insight into the molecule's structure and bonding. From ab initio calculations, Koch and Popelier[15] proposed eight topological criteria for the presence of a hydrogen bond. While these criteria have been found to be valid for the vast majority of hydrogen-bonding complexes between donor and acceptor moieties in their equilibrium geometries, comparatively little is known about how these properties evolve as the donor−acceptor distance (*R*) is varied. Pacios and co-workers studied the topological properties at the B3LYP/6-311++G(d,p) level and MP2/6-311++G(d,p) level, as a function of *R*, on intermolecular, singly hydrogen-bonded systems such as (HF)$_2$, (H$_2$O)$_2$, and water−methanol complexes, and on intermolecular, doubly hydrogen-bonding systems in a cyclic arrangement, such as formic acid dimer, formamide dimer, and the formamide/

formic acid complex.[16−20] Espinosa et al. also studied the very strong hydrogen bond in HF$_2^−$ as a function of the F···F distance at the MP2/6-311++G** level.[21] From these calculations, despite the diversity of hydrogen bonds studied, several common themes emerged. (1) As the donor/acceptor fragments are brought together from infinite separation and approach "typical" hydrogen-bonding distances, the topological properties of the complex exhibit the characteristic values associated with hydrogen bonding, consistent with the Popelier criteria. (2) However, these criteria are nevertheless satisfied for a wide range of donor−acceptor distances, even relatively far from equilibrium. (3) In general, extrema in the topological properties do not correspond to equilibrium donor−acceptor configurations. (4) As *R* decreases even further, there is a smooth transition from hydrogen bonding to covalent bonding, with no discontinuities recorded in the key topological properties. This can only mean that hydrogen bonds, at least as far as the electron density is concerned, represent a distribution of points along a continuum of bonding interactions.

However, to the best of the author's knowledge, with the exception of one study focusing mainly on energetics,[22] no comprehensive, nonequilibrium topological studies have been conducted on systems containing an OH···O intramolecular hydrogen bond (IHB). It is the primary purpose of this study to extend the topological analysis of hydrogen-bonding systems, as a function of donor−acceptor distance, to intramolecular O−H···O hydrogen bonds. The model compound chosen for this study was the *cis*-enol tautomer of malonaldehyde (Figure 1). Malonaldehyde represents a prominent archetype for the O−H···O IHB. Numerous experimental[23−32] and theoretical[33−50]

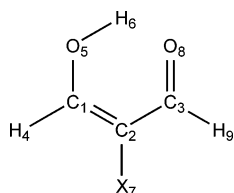† Phone: 541-962-3321. Fax: 541-962-3873. E-mail: jeff.woodford@eou.edu.

Figure 1. Chemical structures of the molecules studied in this work. X = −H, −F, −Cl, −CN, or −NO$_2$.

studies have been devoted to exploring its hydrogen bond, usually with an aim toward understanding the dynamics associated with proton transfer. Certainly, one reason why malonaldehyde has enjoyed intensive theoretical study is because of the availability of a very accurate experimental value for the tunneling splitting[30] and because of its relatively small size, enabling advanced theoretical methods to be applied.

It should be noted that there is some controversy with regards to the use of AIM as a diagnostic tool for understanding bonding interactions.[51,52] The application of AIM to certain interactions has led to counterintuitive results, such as "hydrogen−hydrogen bonding" between ortho hydrogen atoms in biphenyl[53] and carbon−helium "bonding" in the He@adamantane inclusion complex.[54] Nevertheless, since AIM is in common use for categorizing such phenomena, especially hydrogen bonding,[55] it is important that the results be properly calibrated to include as many different categories of hydrogen bonds as do reasonably exist, including intramolecular hydrogen bonds.

Malonaldehyde is also a representative member of a class of compounds containing a resonance-assisted hydrogen bond (RAHB). First proposed by Gilli et al.,[56,57] the RAHB model suggests that π-electron delocalization between the donor and acceptor atoms, via the carbon atom π framework, is responsible for enhancing the strength of malonaldehyde's IHB. Because the AIM methodology enables the calculation of individual atomic properties such as total electronic charge, another purpose of this study is to examine in greater detail the RAHB effect by using AIM-derived results upon hydrogen bond formation.

Finally, while the focus of the study is on malonaldehyde, to examine the substituent effect on the hydrogen bond, four α-substituted derivatives of malonaldehyde were also chosen for study: the fluoro, chloro, cyano, and nitro derivatives. These were chosen because they are symmetric with respect to the hydrogen bond, thereby enabling the donor and acceptor oxygen atoms to remain equivalent in terms of proton affinity. It has been known for quite a while that strong hydrogen bonds tend to result when the donor and acceptor atoms have equal proton affinities. While Lluch et al. have shown that this is not an absolute requirement,[58] nevertheless, the complications arising from proton affinity mismatch have been eliminated from this study, thereby enabling the effect of the substituent to be on the hydrogen bond as a whole, and not on the donor or acceptor atom specifically.

Theoretical Methods

All electronic structure calculations were performed employing density functional theory (DFT), using the B3LYP functional[59−61] and the 6-311++G(2d,p) basis set, as implemented in the GAMESS ab initio software package.[62] The DFT integration grid employed was $r = 96$, $\theta = 36$, and $\phi = 72$. To locate the equilibrium structures of the molecules studied in this work, geometries were optimized until each member of the gradient vector fell to less than 10^{-6} au. A normal-mode analysis was conducted to confirm the absence of imaginary frequencies; this was conducted seminumerically by displacing each atom

by ± 0.01 bohr along each dimension, calculating the gradient analytically, and then numerically constructing the Hessian matrix. The same procedure was used for both the *trans*-enol and *cis*-enol conformers. For the constrained optimizations, the molecule was oriented such that O$_5$ was situated at the origin and O$_8$ was on the positive *x*-axis; the coordinates of these two atoms were held fixed while the rest of the molecule was allowed to relax. In a constrained optimization, false minima can sometimes emerge; therefore, for each optimization, the gradient vector was examined to ensure that the *x*-component of the gradient vector for O$_5$ was exactly equal and opposite to the *x*-component of the gradient vector for O$_8$, with all other values at or below the 10^{-6} au threshold. This ensured that the rest of the molecule was indeed fully relaxed. Topological properties were calculated with the AIMPAC suite of programs.[63] For the integrated atomic properties, the Laplacian (*L*) must equal zero due to the zero-flux boundary condition; therefore, its calculation on a real grid represents an estimate of integration error. For all atoms other than H$_6$, *L* was 10^{-4} au or lower; integration over the atomic basin of H$_6$ proved more challenging because of its involvement in hydrogen bonding. A finer grid was used for its integration, but even still, *L* sometimes approached 10^{-3} au. All calculations were performed either on a networked cluster of 24 Pentium IV computers running Linux or on a 12-node parallel processing server running Beowulf Linux, both maintained by the Department of Computer Science and Multimedia Studies at Eastern Oregon University.

Results and Discussion

Equilibrium Structural Properties. Shown in Table 1 is a comparison of selected structural properties of the equilibrium structure of malonaldehyde calculated in this work with previous theoretical results, along with experimental values. Because of the wealth of published theoretical work available for malonaldehyde, only data from comparable levels of theory (e.g., triple-ζ basis sets with polarization and diffuse functions, inclusion of dynamic correlation) were chosen for comparison. One can see that the present results are in excellent agreement with prior results, although the results of ref 64 are a significant outlier. The calculated values for malonaldehyde are also in substantial agreement with experiment; bond lengths do not differ by more than 0.02 Å (with the exception of the O−H bond length, for which the experimental result is known to be in error[65]) and valence angles do not differ by more than 0.6°. In Table 2 is presented the same structural data for all of the malonaldehyde derivatives in their equilibrium structures studied in this work. Unlike malonaldehyde, its α-substituted derivatives have received scant theoretical attention. α-Fluoromalonaldehyde has been studied previously by Picherri[40] at the B3LYP/cc-pVTZ level; α-chloromalonaldehyde has been studied by Nishimura et al.[66] at the semiempirical level; both α-fluoro- and α-chloromalonaldehyde have been studied by Grabowski[38] at the MP2/6-311++G** level; and α-nitromalonaldehyde has been studied by Tayyari et al.[67] at the B3LYP/6-311++G** level and by Buemi and Zuccarello[68] at the B3LYP/6-31G** level. To the author's knowledge, α-cyanomalonaldehyde has not been theoretically studied previously. The present results are in excellent agreement with the previous density functional results, while the MP2 method tends to overestimate bond lengths compared to the B3LYP method.

From the structural data, it is evident that the monohalogenated derivatives possess structural characteristics less favorable for hydrogen bonding, while the cyano and nitro derivatives have shorter O···O distances and elongated O−H bonds

TABLE 1: Comparison of Selected Structural Properties of the Equilibrium Structure of the *cis*-Enol Tautomer of Malonaldehyde with Published Work of a Similar Theoretical Level and with Experiment[a]

method	r(C−C)	r(C=C)	r(C−O)	r(C=O)	r(O−H)	r(H···O)	r(O···O)	α(CCC)	α(C=C−O)	α(C−C=O)	α(C−O−H)	ref
MP2/ 6-311G**	1.444	1.365	1.322	1.239	0.991	1.678	2.581					33
MP2/ 6-311G**					0.991	1.682	2.585		124.4		104.7	37
MP2/ 6-311++G**	1.445	1.367	1.324	1.242	0.992	1.687	2.585					38
BLap1/ TZVP	1.431	1.363	1.328	1.250	1.001	1.697	2.595	120.2	123.9	123.6	105.3	50
PLap1/ TZVP	1.435	1.362	1.336	1.251	0.996	1.760	2.638	120.9	124.4	123.8	105.5	50
B3LYP/ TZ2P	1.434	1.362	1.318	1.239	1.002	1.656	2.559	119.4	123.8	123.4	105.8	35
B3LYP/ cc-Pvtz	1.434	1.361	1.317	1.237	1.000	1.673	2.571	119	124	124	106	40
B3LYP/ 6-311G**	1.437	1.368	1.319	1.245	1.007	1.641	2.554	118.9	123.9	123.4		67
B3LYP/ 6-311+G(2d,p)	1.43	1.36	1.32	1.24	1.002	1.670	2.570		123.9		106.1	37
B3LYP/ 6-311++G**	1.438	1.364	1.319	1.238	0.997	1.7	2.587	119.7	124.2	123.3		67
B3LYP/ 6-311++G**	1.457	1.341	1.349	1.214	0.962							64
B3LYP/ 6-311++G(2d,p)	1.435	1.362	1.318	1.239	1.002	1.673	2.572	119.6	123.9	123.4	106.2	b
experiment	1.454	1.348	1.320	1.234	0.969	1.68	2.553	119.4	124.5	123.0	106.3	24

[a] Distance values are in angstroms; angles are in degrees. [b] This work.

TABLE 2: Selected Structural Properties of the *cis*- and *trans*-Enol Conformers of the Five Molecules Studied in This Work[a]

conformer	−X	r(C−C)	r(C=C)	r(C−O)	r(C=O)	r(O−H)	r(H···O)	r(O···O)	α(CCC)	α(C=C−O)	α(C−C=O)	α(C−O−H)	α(OHO)
cis-enol	−H	1.435	1.362	1.318	1.239	1.002	1.673	2.572	119.6	123.9	123.4	106.2	146.9
	−F	1.434	1.355	1.324	1.234	0.994	1.740	2.618	122.6	123.0	122.0	107.0	145.0
	−Cl	1.440	1.361	1.319	1.234	0.998	1.695	2.582	120.9	123.3	122.2	106.9	145.8
	−CN	1.451	1.375	1.305	1.232	1.006	1.643	2.547	119.1	123.4	122.4	106.8	147.0
	−NO₂	1.444	1.372	1.302	1.234	1.010	1.632	2.541	120.8	122.4	120.9	106.8	147.3
trans-enol	−H	1.463	1.344	1.343	1.214	0.964		2.890	126.7	124.1	126.3	110.1	
	−F	1.462	1.341	1.345	1.211	0.964		2.929	129.7	123.0	125.0	109.8	
	−Cl	1.471	1.345	1.342	1.209	0.964		2.841	127.0	123.0	124.4	109.8	
	−CN	1.485	1.357	1.329	1.207	0.965		2.810	125.1	123.3	124.8	110.5	
	−NO₂	1.477	1.354	1.324	1.210	0.966		2.795	126.4	122.9	122.9	110.3	

[a]Distances are in angstroms; angles are in degrees.

TABLE 3: Selected Calculated Harmonic Vibrational Frequencies Associated with the IHB and a Comparison to Experiment[a]

mode description	−H	−H(exptl)[b]	−F	−Cl	−CN	−NO₂
O···O stretch	275	282	251	268	284	291
OH wag	928	873	863	895	944	967
	1015	981	974	991	1021	1069
OH bend	1387	n/a	1403	1382	1397	1394
	1626		1619	1612	1622	1633
OH stretch	3107	2856	3177	3164	3049	2991
	3171	2960	3265	3209	3177	

[a] All values are in cm⁻¹. [b] References 25 and 69.

compared to those of unsubstituted malonaldehyde, thereby implying stronger hydrogen bonds. From the structural data on the IHB ring bonding, it is evident that the cyano and nitro derivatives also possess more symmetric CC and CO bonding, which is also consistent with the RAHB model of Gilli et al.[56] Finally, the OHO valence angle is not much changed upon substitution, varying only by 2.3° among the compounds studied, as its value is determined primarily by the rigid framework imposed by the six-membered ring instead of by hydrogen bond stabilization.

Equilibrium Harmonic Vibrational Frequencies. The calculated harmonic vibrational frequencies associated with the IHB for malonaldehyde and its derivatives are presented in Table 3, along with the available experimental frequencies for malonaldehyde[25] as reassigned in a recent theoretical study.[69] Agreement with the available experimental data is good, considering that calculated harmonic vibrational frequencies tend to overestimate the experimental values, with the exception of the OH and O···O stretching frequencies due to their strong anharmonicity. It should be noted that there is significant resonant coupling among many of the modes associated with the hydrogen bond; ν(OH) experiences strong resonant coupling with the enolic CH stretch; and the OH bending and wagging modes are also strongly coupled to CH bending and wagging

modes, respectively. For this reason, two numbers are listed for each of these three modes, with the exception of ν(OH) for nitromalonaldehyde. For this molecule, ν(OH) is so red-shifted that its frequency is below even that of a typical CH stretch, and the two modes are no longer significantly resonantly coupled.

As is well-known in the case of intermolecular hydrogen bonds, formation of a hydrogen bond tends to give rise to a red-shift of the ν(OH) stretching frequency, compared to a "typical" OH stretch, with larger red-shifts corresponding to stronger hydrogen bonds.[70,71] The situation is necessarily more complex for intramolecular hydrogen bonds, as ν(OH), as well as other vibrational modes, are strongly coupled to many other vibrational modes of the molecule, including ones associated with the acceptor. However, upon inspection of Table 3, we see that if malonaldehyde is used as a reference point, the same qualitative trends for intermolecular hydrogen bonds remain valid for the intramolecular case. For instance, the red-shift of the ν(OH) frequencies for cyanomalonaldehyde and nitromalonaldehyde are larger than those of fluoromalonaldehyde and chloromalonaldehyde, which suggests that these IHBs are stronger than the others, consistent with the structural data of Table 2. Similarly, the OH wagging frequencies for fluoromalonaldehyde and chloromalonaldehyde are less blue-shifted than those of cyanomalonaldehyde and nitromalonaldehyde, which is also consistent with these latter two molecules possessing stronger IHBs: as the IHB strength increases, one would expect the hydrogen atom vibrations transverse to the hydrogen-bonding plane to become "stiffer", hence the force constants and the vibrational frequencies should increase.

Equilibrium Energetics. Shown in Table 4 is a summary of the apparent energy of the hydrogen bond for the five molecules considered in this work. Unlike the case of intermolecular hydrogen bonds, there is no unique definition for the energy of an intramolecular hydrogen bond. Many authors have

TABLE 4: Calculated Estimates of the Intramolecular Hydrogen Bond Energy for the Five Molecules Studied in This Work[a]

| −X	$E_{HB}^{(1)}$	$E_{HB}^{(2)}$	$E_{HB}^{(3)}$	$E_{HB}^{(4)}$	$E_{HB}^{(5)}$
−H	13.0	13.1	15.8	9.8	13.9
−F	11.0	11.8	12.6	5.1	11.5
−Cl	12.0	12.0	14.7	4.9	13.3
−CN	12.6	12.5	17.4	8.7	15.4
−NO$_2$	12.8	12.9	18.0	8.2	15.8

[a] All values are in kcal/mol.

devised various methods to estimate the energy of an intramolecular hydrogen bond; the methods adopted in this work are as follows.

1. Cis/Trans Analysis. In this method, the energy of the hydrogen bond is taken to be the difference in energy between the *trans*-enol, nonchelated form and the *cis*-enol, chelated form, or ΔE of the following reaction.[34,43]
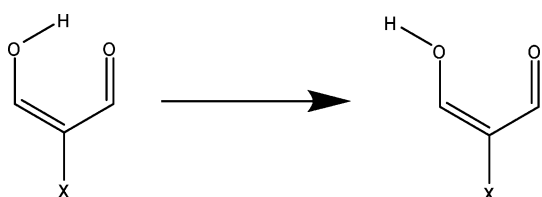
$$E_{HB}^{(1)} = \Delta E = E_{trans} - E_{cis}$$

2. Isodesmic Reactions. In this method, the energy of the hydrogen bond is determined from ΔE of a suitable isodesmic reaction, such as the following.[72]
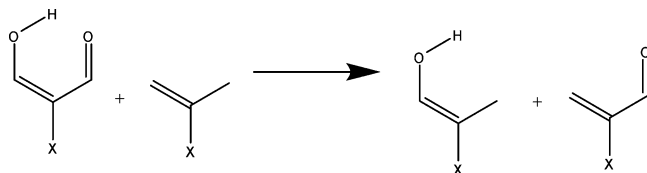
$$E_{HB}^{(2)} = \Delta E_{isodesmic}$$

3. Local Potential Energy Density. In this method, the energy of the hydrogen bond is equal to one-half of the local potential energy density at the hydrogen bond critical point multiplied by the atomic volume element a_0^3.[73]

$$E_{HB}^{(3)} = -\frac{a_0^3}{2} V_{CP}$$

4. Conformational Analysis. In this method, the energy of the hydrogen bond is determined from a complex conformational analysis involving the four possible conformers (ZZ, EZ, ZE, EE) resulting from rotation of the donor and acceptor groups.[74] The ZZ conformer is the lowest energy *cis*-enol form; the EZ and ZE conformers are formed by rotation of the donor and acceptor, respectively, about their respective carbon−carbon bonds; and the EE conformer is formed by rotation of both the donor and the acceptor about their bonds. Using the notation of ref 74, the energy of the hydrogen bond is given as follows.

$$E_{HB}^{(4)} = \frac{1}{2}(E^{EZ,f} + E^{EE,f}) - E^{ZZ}$$

In this equation, $E^{EZ,f}$ ($E^{EE,f}$) is the energy of the fictitious EZ (EE) conformer in which the bond lengths are the same as in

the ZZ conformer; and E^{ZZ} is the energy of the ZZ conformer in its equilibrium configuration.

5. Empirical Energy−Geometry Correlations. Many authors have attempted to establish correlations between energetic and geometric properties of the intramolecular hydrogen bond; the one that appears to be the most robust is the exponential correlation recently found by Musin and Mariam[75] in their detailed examination of a number of IHB compounds, including some considered in this study, given below.

$$-E_{HB}^{(5)} = (-5.554 \times 10^5) \exp(-4.12R)$$

In this equation, R is the O···O distance in angstroms and E_{HB} is in kilocalories per mole. The negative sign appears before E_{HB} because, in ref 75, the hydrogen bond energy is defined as a negative number while in this work it is defined as a positive number.

As shown in Table 4, there are significant differences between the five methods for the compounds studied in this work. Methods 1 and 2, based on ΔE values of pseudochemical reactions, predict that all five molecules should have roughly the same hydrogen bond energies, while Methods 3 and 5, based solely on the properties of the individual IHB molecule itself, predict that the fluoro and chloro derivatives should have weaker hydrogen bonds, and the nitro and cyano derivatives should have stronger hydrogen bonds, as compared to malonaldehyde, consistent with the structural data. Method 4 appears to grossly underestimate the hydrogen bond energy as compared to the other methods.

While numerous crystallographic and spectroscopic studies tend to suggest that stronger *intermolecular* hydrogen bonds are generally associated with shorter O···O distances, longer O−H bonds, shorter H···O contacts,[76,77] and red-shifted ν(OH) frequencies,[71] the trend is not so clear-cut for *intramolecular hydrogen bonds.* Korth et al. found that for a series of substituted phenols, there is no clear correlation between the energy of an intramolecular hydrogen bond and these "typical" features used to identify the presence of a hydrogen bond.[78] The present study also supports the conclusion by Korth et al. that Method 1, the cis/trans method, cannot be used to unequivocally distinguish between strong and weak IHBs. Nevertheless, the preponderance of the evidence clearly suggests that cyanomalonaldehyde and nitromalonaldehyde, containing strong electron-withdrawing groups, have stronger IHBs than the others. This result was also found by Korth et al.[78] by use of solute acidity/solvent basicity parameters obtained from Abraham et al.[79]

Nonequilibrium Structural Properties. Presented in Table 5 is a selection of structural properties of malonaldehyde resulting from its constrained optimization as R is varied. The corresponding data for the other four molecules are given as Tables S1−S4 in the Supporting Information. From the data, one may plainly see that as far as the hydrogen bond is concerned, there are two distinct regions: At very short R, the hydrogen bonding is symmetric. At $R_{trans} \approx 2.24$ Å, the hydrogen bonding undergoes a transition and becomes asymmetric, with different values for the O−H and H···O distances. These values then vary smoothly as R increases further. Figure 2 shows the r(O−H) and r(H···O) distances plotted as a function of R; one can plainly see the quasilinear increase in r(H···O) vs R as $R \gg R_{trans}$. It is interesting to note that the O−H distance remains larger than that of the non-hydrogen-bonded *trans*-enol tautomer, even for donor−acceptor distances as long as 3.3 Å. This means that the impact of hydrogen bonding is nonnegligible even for such long distances. The other structural properties also reflect this general division into two regions: at $R < R_{trans}$, the other

Intramolecular H Bonding in Derivatives of Malonaldehyde

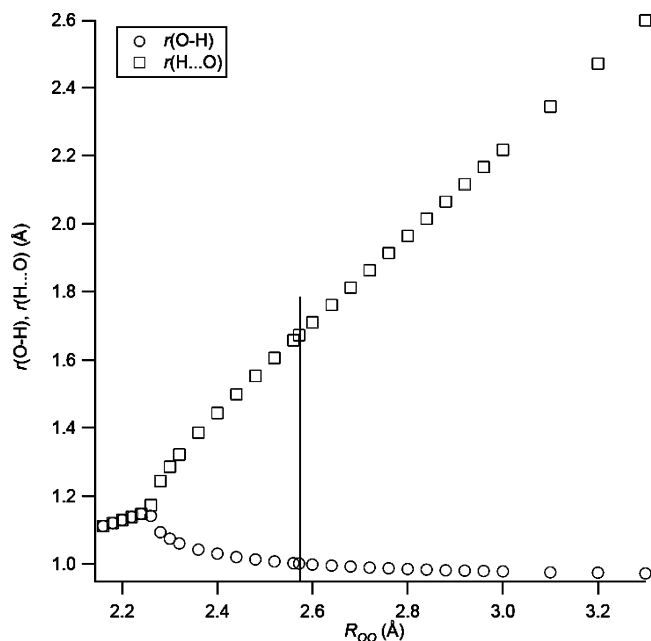*J. Phys. Chem. A, Vol. 111, No. 34, 2007* **8523**

Figure 2. The O–H and H···O distances in malonaldehyde as a function of the O···O distance. The solid vertical line represents the equilibrium structure.

TABLE 5: Selected Structural Properties of Malonaldehyde Obtained from Constrained Optimization after Holding the O···O Distance (R) Fixed[a]

R	$r(C-C)$	$r(C=C)$	$r(C-O)$	$r(C=O)$	$r(O-H)$	$r(H\cdots O)$	$\alpha(OHO)$
2.16	1.393	1.393	1.274	1.274	1.112	1.112	152.3
2.18	1.393	1.393	1.274	1.274	1.121	1.121	153.0
2.20	1.394	1.394	1.275	1.275	1.130	1.130	153.5
2.22	1.394	1.394	1.275	1.275	1.139	1.139	154.0
2.24	1.394	1.394	1.275	1.275	1.148	1.148	154.5
2.26	1.397	1.392	1.278	1.273	1.142	1.173	154.8
2.28	1.405	1.384	1.287	1.265	1.094	1.244	154.3
2.30	1.410	1.381	1.292	1.260	1.075	1.286	153.8
2.32	1.413	1.378	1.295	1.257	1.061	1.322	153.3
2.36	1.418	1.374	1.301	1.252	1.043	1.386	152.4
2.40	1.422	1.370	1.305	1.249	1.031	1.444	151.4
2.44	1.426	1.368	1.309	1.246	1.021	1.499	150.4
2.48	1.429	1.366	1.312	1.243	1.014	1.553	149.3
2.52	1.432	1.364	1.315	1.241	1.008	1.606	148.3
2.56	1.434	1.362	1.317	1.239	1.003	1.658	147.2
2.60	1.436	1.361	1.319	1.237	0.999	1.710	146.2
2.64	1.439	1.360	1.321	1.236	0.996	1.761	145.1
2.68	1.441	1.359	1.323	1.234	0.993	1.812	144.1
2.72	1.442	1.358	1.325	1.233	0.990	1.863	143.1
2.76	1.444	1.357	1.326	1.232	0.988	1.914	142.0
2.80	1.446	1.357	1.328	1.231	0.986	1.964	141.0
2.84	1.447	1.356	1.329	1.229	0.984	2.015	140.0
2.88	1.449	1.356	1.330	1.228	0.982	2.065	139.0
2.92	1.450	1.355	1.331	1.228	0.981	2.116	138.0
2.96	1.452	1.355	1.332	1.227	0.980	2.167	137.0
3.00	1.453	1.355	1.333	1.226	0.979	2.217	136.1
3.10	1.457	1.354	1.335	1.224	0.976	2.344	133.7
3.20	1.461	1.354	1.337	1.223	0.975	2.470	131.5
3.30	1.464	1.355	1.338	1.221	0.973	2.597	129.3

[a] Distances are in angstroms; angles are in degrees.

bonds in the molecule adopt symmetric values appropriate for C_{2v} symmetry. This indicates that the O–H–O bonding interaction in this region may truly be regarded as a 3-center, 4-electron bond. For $R > R_{trans}$, the symmetry is broken and the molecule reverts to C_s symmetry, which is found for the equilibrium structure. The transition from symmetric to asymmetric hydrogen bonding appears at approximately the same donor–acceptor distance for all five molecules studied. The hydrogen bonding angle, $\alpha(OHO)$, also reaches a maximum near R_{trans}; at distances larger than this, the angle decreases as the
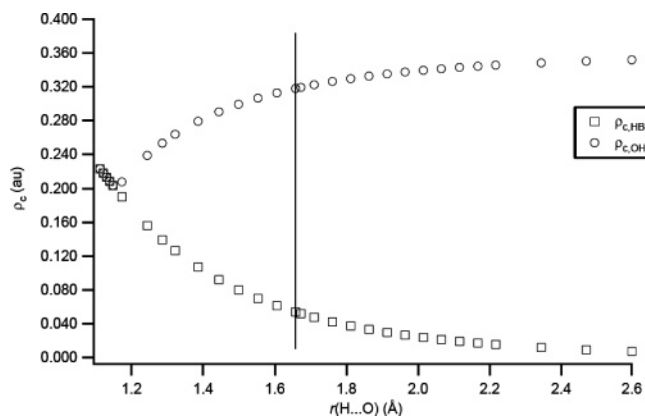

Figure 3. The electron density at the bond critical point for the hydrogen bond and the O–H bond in malonaldehyde as a function of r. The solid line represents equilibrium values.

hydrogen bond interaction becomes weaker. And at distances shorter than this, the hydrogen atom avoids repulsive interactions by moving perpendicular to the O···O line, thereby diminishing $\alpha(OHO)$. It should also be noted that the donor–acceptor distance corresponding to the symmetric–asymmetric hydrogen-bonding transition, 2.24 Å, is exceptionally short and that no neutral intramolecular O–H···O system has yet been discovered with an equilibrium donor–acceptor distance that small.

Equilibrium and Nonequilibrium Topological Properties. As demonstrated by Bader and co-workers, there are two general categories of topological properties: those which are defined at specific points in the electron density (local properties)[74] and those which may be acquired by integrating the electron density over a region of zero flux, corresponding to atomic properties. In this study, first data associated with topological properties at critical points will be discussed, followed by integrated properties over atomic basins.

A. Local Properties. The electron density at a bond critical point (ρ_c) is a key topological descriptor of internuclear interactions, particularly hydrogen bonds. The Popelier criteria for hydrogen bond formation include the requirement that ρ_c for a hydrogen bond ($\rho_{c,HB}$) be within the range of 0.002–0.040 au. Shown in Figure 3 are plots of $\rho_{c,HB}$ and the electron density at the O–H bond critical point ($\rho_{c,OH}$) versus r, the hydrogen bond distance. The numerical values for these data for all molecules are given as Tables S5–S9 in the Supporting Information. The general shape of the $\rho_{c,HB}$ curve in Figure 4 is that of exponential decay, consistent with recent findings.[17,80–89] The first emergence of a hydrogen bond critical point appears at $r = r(H\cdots O) \approx 2.60$ Å; as r decreases, $\rho_{c,HB}$ reaches the minimum threshold for hydrogen bonding, becoming equal to 0.002 au only at $r \approx 2.09$ Å. Similarly, in this region, $\rho_{c,OH}$ is only slightly less than its value in the *trans*-enol form (0.363 au). As r decreases further, $\rho_{c,HB}$ increases and $\rho_{c,OH}$ decreases, as one would intuitively expect; $\rho_{c,HB}$ surpasses the maximum Popelier threshold for hydrogen bonding, 0.040 au, at $r \approx 1.79$ Å. Notably, this occurs at an internuclear separation greater than that of the equilibrium structure ($r = 1.67$ Å); at equilibrium, $\rho_{c,HB} = 0.052$ au. However, most peculiar are the behaviors of $\rho_{c,HB}$ and $\rho_{c,OH}$ at very short internuclear separations. At $r = r_{trans} = 1.15$ Å, the two curves coalesce into a single curve. The plot of $\rho_{c,HB}$ vs r remains continuous throughout; however, this transition between symmetric and asymmetric bonding is manifested as a discontinuity when $\rho_{c,OH}$ is plotted vs r. Thus, while the present results validate the findings of Pacios and co-workers,[16,17] who found a continuous transition from hydrogen bonding to covalent bonding when $\rho_{c,HB}$ is plotted versus r, the
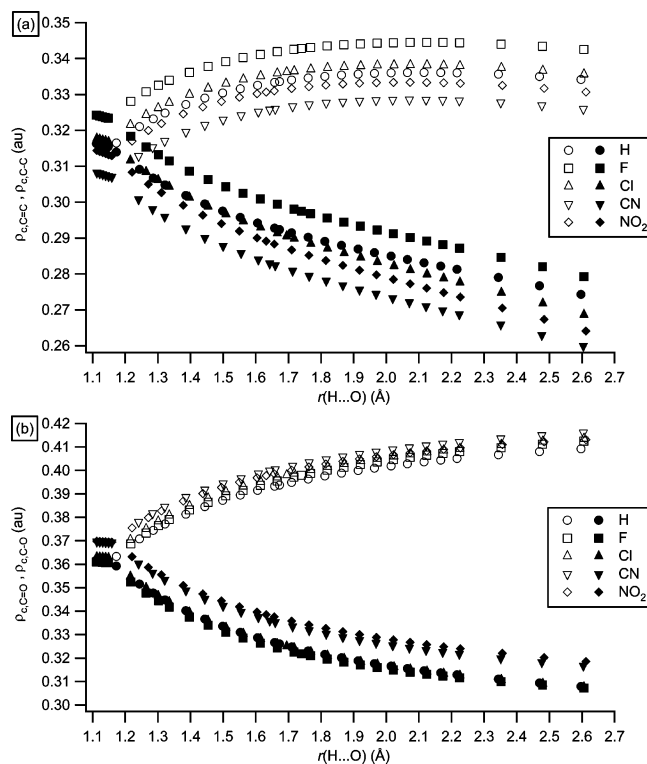
Figure 4. Variation of the electron density of the bond critical points for the (a) carbon−carbon and (b) carbon−oxygen bonds in the five molecules studied in this work. Open symbols represent the double-bond critical point; filled symbols represent the single-bond critical point.

TABLE 6: Fitting Parameters for $\rho_{c,HB}$ to a Simple Exponential Function of Hydrogen Bond Distance and Comparison to Literature Values[a]

−X	y_0 (au)	A (au)	b (Å^{-1})	ref
−H	0.00474 ± 0.00036	4.49 ± 0.10	2.73 ± 0.02	b
−F	0.00443 ± 0.00031	4.29 ± 0.09	2.69 ± 0.02	b
−Cl	0.00443 ± 0.00032	4.33 ± 0.09	2.70 ± 0.02	b
−CN	0.00486 ± 0.00039	4.59 ± 0.11	2.74 ± 0.02	b
−NO$_2$	0.00486 ± 0.00039	4.57 ± 0.10	2.74 ± 0.02	b
	0.001	4.4	2.7	84
		2.71	2.40	85
		9.62 ± 4.00	3.2 ± 2.0	87
		2.87 ± 0.43	2.32 ± 0.10	88
		1.559	2.113	89

[a] Error estimates represent one standard deviation. [b] This work.

topological data still reveal a specific point at which the hydrogen bond becomes symmetric and therefore purely covalent. The fitting coefficients for the $\rho_{c,HB}$ vs r fit to a simple exponential function of the form $y(x) = y_0 + A \exp(-bx)$, with $y(x) = \rho_{c,HB}$ and $x = r$, are given in Table 6; only data points with $r > r_{trans}$ were used in the fit. The fitted data are in good agreement with the results obtained in ref 84, although such agreement must be considered fortuitous as there is a great deal of scatter in the reported literature.

A near-negligible dependence on the nature of the substituent is manifested in the data of Table 6, as both A and b remain nearly constant for all five compounds. Indeed, when plotted, the five curves visually appear to superimpose on one another. Thus, the present findings support the conclusion that the electron density at the hydrogen bond critical point is a very local property, largely independent of the nature of the hydrogen bond itself; different values for $\rho_{c,HB}$ arise due to different donor−acceptor distances, and not necessarily from an intrinsically stronger or weaker hydrogen bond. This finding is
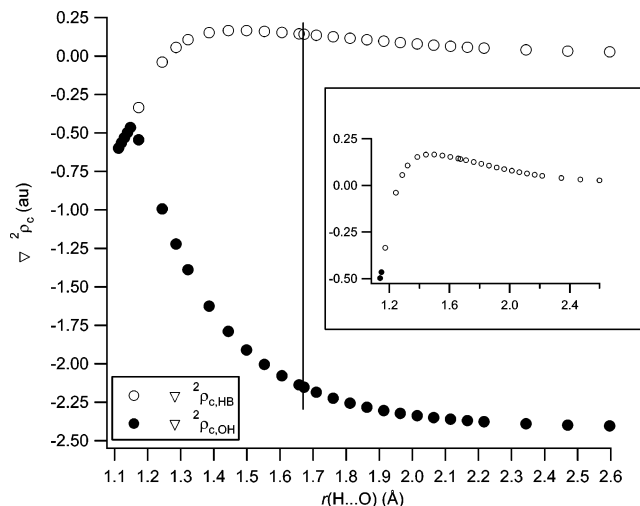
consistent with the work of Alkorta et al.,[90] who found that the electron density at the hydrogen bond critical point is an additive property for a large number of complexes; one would only expect additivity if the nonlocal influences on the interactions are minimal. This is also consistent with the work of Grabowski,[91] who found by factor analysis that the dependency of the hydrogen bond interaction energy on various geometric and topological properties may be explained to a large extent by only one factor. Here, it is shown how $\rho_{c,HB}$ and r are linearly dependent.

The variation of ρ_c for the other bonds in the IHB ring is presented in Figure 4, parts a and b. The top figure displays the data for the C−C and C=C bonds; the bottom figure displays the data for the C−O and C=O bonds. Both figures are qualitatively similar: the double bond has larger ρ_c values than the single bond, and as r decreases, both curves converge to the same point at $r = r_{trans}$. The carbon−carbon bonds appear to be much more strongly affected by the nature of the α-substituent than the carbon−oxygen bonds. Indeed, for the carbon−oxygen bonds, only $\rho_{c,C−O}$ is noticeably affected: $\rho_{c,C−O}$ values for the nitro and cyano derivatives are systematically higher than $\rho_{c,C−O}$ values for the other three compounds.

The Laplacian of the electron density at a bond critical point ($\nabla^2 \rho_c$) is another sensitive measure of the properties of a chemical bond. Positive values of $\nabla^2 \rho_c$ indicate local depletion of electron density, or a closed-shell (CS) interaction, while negative values of $\nabla^2 \rho_c$ indicate local concentration of electron density, or a shared-shell (SS) interaction. The Popelier criteria for hydrogen bonding require that the value of the Laplacian at the hydrogen bond critical point ($\nabla^2 \rho_{c,HB}$) should be between 0.02 and 0.15 au. Shown in Figure 5 are plots of $\nabla^2 \rho_{c,HB}$ and $\nabla^2 \rho_{c,OH}$ vs r. We note the same qualitative behavior as in the case of ρ_c: as the oxygen atoms are well separated, $\nabla^2 \rho_{c,OH}$ is strongly negative, indicating an isolated covalent bond, and $\nabla^2 \rho_{c,HB}$ is just barely above zero. However, even for $r = 2.6$ Å, $\nabla^2 \rho_{c,HB}$ exceeds the minimum Popelier criterion for hydrogen bonding. Unlike the case for $\rho_{c,HB}$, however, $\nabla^2 \rho_{c,HB}$ remains, more or less, within the range of 0.02−0.15 au throughout the weak- to intermediate-strength hydrogen-bonding region, reaching a value of 0.141 au at equilibrium and a maximum value of 0.165 au at $r = 1.5$ Å. Consistent with the findings of Pacios and co-workers,[16,17] the maximum value of $\nabla^2 \rho_{c,HB}$ does not correspond to the equilibrium configuration of malonaldehyde.

Figure 5. The Laplacian of the electron density at the bond critical point for the hydrogen bond and the O−H bond in malonaldehyde. Inset: An enhanced view of the Laplacian between −0.50 and +0.25 au. The solid vertical line represents equilibrium values.

Intramolecular H Bonding in Derivatives of Malonaldehyde

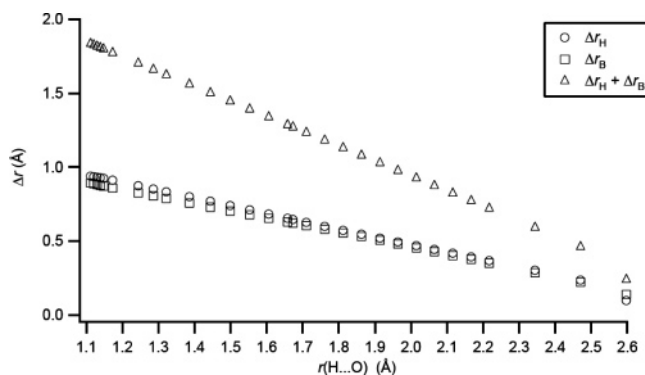*J. Phys. Chem. A, Vol. 111, No. 34, 2007* **8525**

Figure 6. Change in the radius of the hydrogen and acceptor oxygen atom for the hydrogen bond in malonaldehyde.

Once past the maximum, $\nabla^2\rho_{c,HB}$ then falls sharply, and $\nabla^2\rho_{c,OH}$ rises sharply, until $r = r_{trans}$, when the two curves coalesce into a single curve and the hydrogen bond becomes symmetric. Upon further shrinking of the O···O distance, both $\nabla^2\rho_{c,HB}$ and $\nabla^2\rho_{c,OH}$ sharply decrease, with values of about one-fifth of the value for the covalent O−H bond.

A further requirement for hydrogen bonding, which is described by Koch and Popelier as the only one sufficient for predicting the presence of a hydrogen bond,[15] is that the hydrogen atom and the acceptor atom must mutually penetrate. Quantitatively, this means that the bonded radius of the hydrogen atom (r_H) and of the acceptor oxygen atom (r_B) must each be smaller than the corresponding nonbonded radii, r_H^0 and r_B^0, or that $\Delta r_X = r_X^0 - r_X > 0$ for X = H and B. The bonded radius of an atom is taken to be the distance from the nucleus to the bond critical point, and the nonbonded radius of an atom is conventionally defined as the distance from the nucleus to the 0.001 au contour of the electron density. In this study, r_H^0 was calculated as the distance from the H_6 nucleus to the 0.001 au contour in the direction of the O_5-H_6 bond in the *trans*-enol conformer; similarly, r_B^0 was calculated as the corresponding distance in the direction of the $C_3=O_8$ bond in the *trans*-enol conformer. As a practical matter, these radii were determined by calculating $\rho(r)$ for 9−12 points in space in the direction of the appropriate bond, and then fitting the results to a decaying exponential as a function of the distance from the nucleus. Presented in Figure 6 are the plots of Δr_H, Δr_B, and $\Delta r_H + \Delta r_B$ vs r for malonaldehyde. The curves for the other four molecules are nearly identical. For all internuclear separations, both Δr_H and Δr_B are positive, indicating the presence of hydrogen bonding throughout. The hydrogen atom and oxygen atom contribute to the penetration in nearly equal amounts. The same result was found by Pacios et al.[16, 17] The curves are linear; a fit of $\Delta r_H + \Delta r_B$ vs r to a straight line yields a slope of −1.01. It is also interesting to note that there does not appear to be a discontinuity in $\Delta r_H + \Delta r_B$ at r_{trans}, indicating that while this criterion is sufficient to establish the presence of a hydrogen bond, it does not appear to be capable of discriminating between symmetric and asymmetric hydrogen bonding.

B. Integrated Properties. The four Popelier criteria[15] for hydrogen bonding involving integrated topological properties include the following: (1) energetic destabilization, (2) loss of charge, (3) reduced volume, and (4) increased polarization of the hydrogen atom, compared to a non-hydrogen-bonded reference species. For purposes of comparison, the *trans*-enol tautomer is taken to be the reference compound of the five molecules studied. It should be noted that Bickelhaupt et al.,[92] in a careful study on methods of partitioning the atomic charges of a molecule, have criticized the use of AIM-based integrated

properties in understanding molecular properties. They found that for simple molecules, the magnitudes of the AIM-derived integrated charges on atoms were in contradiction to well-established chemical reactivity data on these atoms; a similar result was found by Mandado et al.[93] on a study of carbonyl compounds. However, since the present study is more interested in *trends* in molecular properties associated with variation of the donor−acceptor distance, rather than on the quantitative results themselves, the results arising from an AIM partitioning of the molecular space should be generally applicable. Tables S10−S13 of the Supporting Information contain the numerical values associated with these integrated properties.

Shown in Figure 7a is a plot of $\Delta E_H = E_H - E_H^0$, the difference in the integrated total energy of the IHB hydrogen atom (E_H) as compared to the same quantity in the reference compound (E_H^0), for the five molecules studied. For all molecules, $\Delta E_H > 0$, indicating energetic destabilization. For large r, the destabilization is approximately 10−12 kcal/mol; as r decreases, ΔE_H increases almost linearly until it reaches a maximum of 26−33 kcal/mol at $r \approx 1.4$ Å, or at approximately the same value of r corresponding to the maximum value of $\nabla^2\rho_c$. ΔE_H then decreases somewhat until $r = r_{trans}$, at which point ΔE_H falls sharply as the hydrogen atom becomes stabilized in a three-center, four-electron bond. Malonaldehyde has the greatest amount of energetic destabilization, while nitromalonaldehyde, the compound with the strongest hydrogen bond, has the least.

In Figure 7b is presented Δq_H, or the change in the electric charge of the hydrogen atom with respect to the reference compound, defined analogously to ΔE_H. For all five compounds, Δq_H is positive, indicating a greater loss of charge for the hydrogen atom associated with the hydrogen bond as compared to the *trans*-enol reference structure. Δq_H is approximately 0.02e at large hydrogen-bonding distances, rising to a value of 0.06−0.08e until the symmetric−asymmetric transition is reached. At this point, Δq_H rises sharply. The hydrogen atom in malonaldehyde exhibits the greatest loss of charge, while the one in nitromalonaldehyde exhibits the least.

Presented in parts c and d of Figure 7 are $\Delta\mu_H$ and ΔV_H, respectively, for the five compounds studied. The first quantity corresponds to the change in the magnitude of the dipole moment on the hydrogen atom, while the second corresponds to the change in the atomic volume of the hydrogen atom. At large values of r, $\Delta\mu_H$ is very small, owing to its near-spherical shape in the absence of significant hydrogen bonding; as d decreases, $\Delta\mu_H$ decreases rapidly until $r = r_{trans}$, at which point $\Delta\mu_H$ remains fairly constant at approximately −0.12 au. This constancy is to be expected for reasons of symmetry. On the other hand, the change in atomic volume decreases gradually until $r = r_{trans}$, at which point ΔV_H decreases sharply. Again, this is to be expected, as the volume of the hydrogen atom should get more and more "squeezed" as r shrinks. The sharp decrease on the atomic volume at $r < r_{trans}$ is also to be expected, as the acceptor oxygen atom exerts a more profound "squeezing" influence on the hydrogen atom when it is a part of a symmetric hydrogen bond. For these two quantities, no meaningful distinction can be made between the five compounds, as the curves almost superimpose on one another. These quantities, then, appear to be highly local in nature, more so than ΔE_H or Δq_H.

Resonance-Assisted Hydrogen Bonding. The integrated atomic properties provided by the AIM methodology also permit a deeper understanding into the resonance-assisted hydrogen-bonding model. As first explained by Gilli et al.,[56] and later
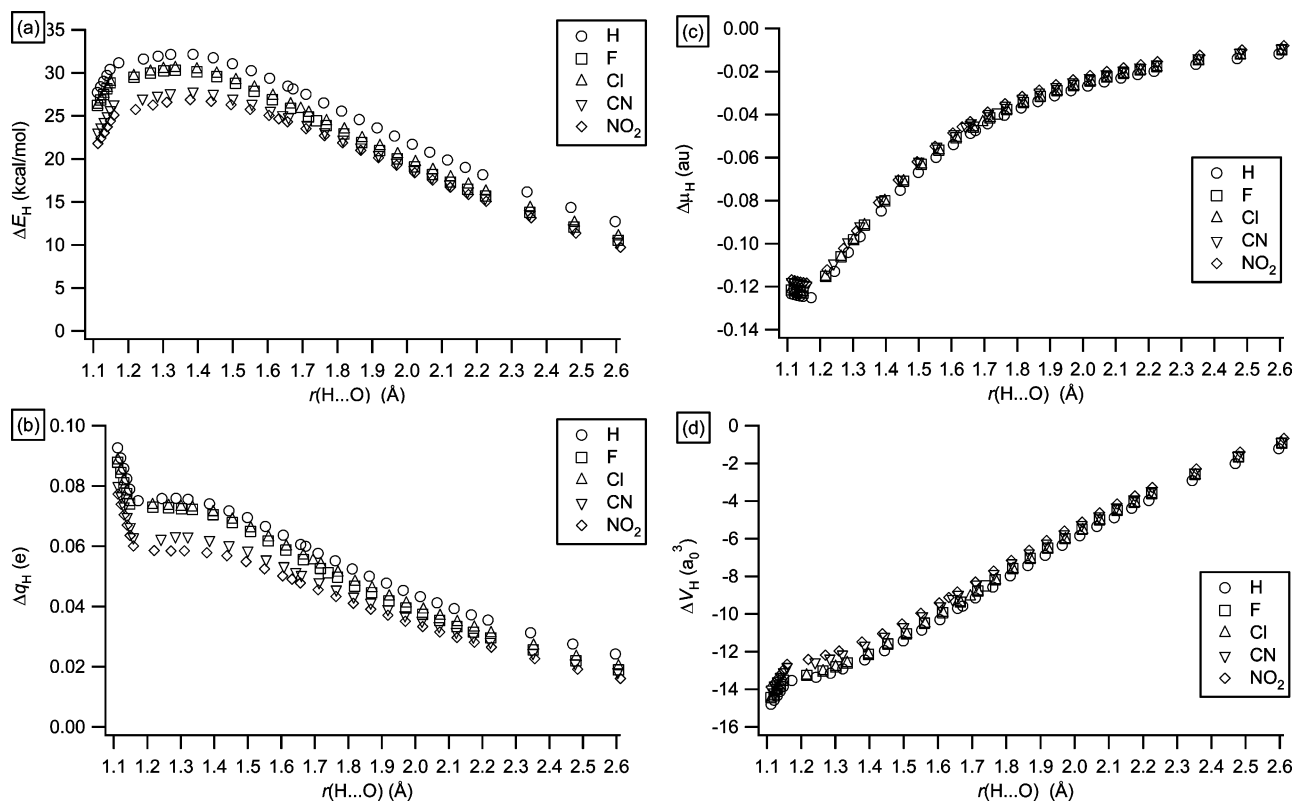
Figure 7. Changes in (a) the integrated atomic energy, (b) the integrated atomic charge, (c) the integrated dipole moment, and (d) the integrated atomic volume of the hydrogen-bond hydrogen atom as compared to the corresponding property in the trans-enol conformer for the five molecules studied in this work.

modified by Madsen et al.,[94] the RAHB effect is a "feedback mechanism that drives the charges in the ring toward symmetry."[94] In other words, the π-conjugated system provides a means by which charge may be redistributed among the two electronegative oxygen atoms in order to maintain electrostatic equilibrium. Therefore, according to the RAHB model, one would expect that as the hydrogen bond distance decreases, the net charges on the IHB ring atoms should undergo significant change, in a symmetric manner, while maintaining overall electroneutrality. Figure 8 depicts a graph of the total integrated charge on the six IHB atoms vs r for malonaldehyde, along with the sum of the charges on the six atoms (also see Supporting Information Table S14). One can see that in malonaldehyde, the total IHB ring charge is negative, between $-0.15e$ and $-0.20e$, indicating that the peripheral hydrogen atoms act as weak charge donors to the IHB ring. Furthermore, there is very little redistribution of charge among the IHB ring atoms as r decreases, with the exception of C_1 and C_3. Notably, the integrated charges on the two oxygen atoms remain almost constant at $-1.1e$ each, even for H···O distances as long as 2.6 Å. As r approaches r_{trans}, the charges for each atom approach their limiting values appropriate for C_{2v} symmetry for the symmetric hydrogen bond. Therefore, it does not appear that there is any significant charge transfer between the OHO hydrogen-bonding moiety and the carbon framework as the hydrogen bond distance decreases.

Wide variations in charge, however, are seen for C_1 and C_3. For long hydrogen bond distances, C_3 has almost one full unit charge, while C_1 has a charge of a little more than $+0.5e$. As r decreases, q_{C3} decreases and q_{C1} increases until both approach their limiting values of $\sim 0.75e$. The variations in charge on these two atoms appear to be equal and opposite; Figure 9 confirms that this indeed is the case. In this figure, q_{C1} is plotted versus q_{C3}; the trend is very nearly linear, with a slope of -0.96.

This indicates that for a unit increase in charge on C_1, there is approximately a unit decrease of charge on C_3, suggesting that the charge lost by one is gained by the other.

For chloromalonaldehyde and cyanomalonaldehyde, the total IHB ring charge is only slightly positive, between $+0.01e$ and $+0.08e$; in these compounds, the chloro and cyano substituents act as weak electronic charge acceptors. Nitromalonaldehyde has an IHB ring charge of between $+0.21e$ and $+0.29e$, indicating the strong electron-withdrawing effect of the nitro substituent. Finally, fluoromalonaldehyde has a large IHB ring charge of about $+0.47e$. This may be attributed to fluorine's strong inductive effect and good overlap between fluorine's $2p_z$ orbital and the π orbitals in the carbon system. While the nitro group's resonant electron withdrawing effect is well-known, its inductive effect is not as strong as fluorine's. Furthermore, similar charge-transfer conclusions may be drawn for these four compounds as for malonaldehyde. For each, q_{C1} and q_{C3} are roughly linearly proportional; the slope of the q_{C1} vs q_{C3} line is -0.84, -0.89, -0.98, and -1.08 for the fluoro, chloro, cyano, and nitro derivatives, respectively. The general trend which emerges is that the compounds exhibiting the strongest hydrogen bonds have the largest degree of charge transfer between C_1 and C_3. This is to be expected, since the strongest hydrogen bonds have the shortest C=C and C−C bonds, thereby enabling greater overlap between the $2p_z$ atomic orbitals on the three carbons and a more fully delocalized π-type HOMO on the three carbons.

An understanding of the nature of the charge redistribution in the IHB ring may be achieved by inspecting the zz-component of the atomic quadrupolar tensor, Q_{zz}, for these six atoms. The atomic quadrupolar tensor measures the asymmetry of the atomic charge density; Q_{zz} examines the magnitude of the π-electron distribution on a particular atomic center. Presented in Table S15 of the Supporting Information, and in Figure 10,
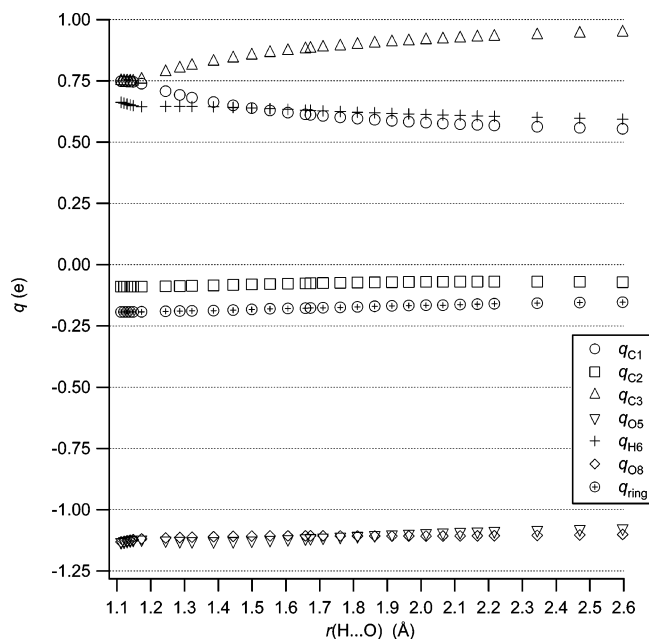
Figure 8. The integrated atomic charges of the six atoms involved in the intramolecular hydrogen bond ring in malonaldehyde, and the total IHB charge.
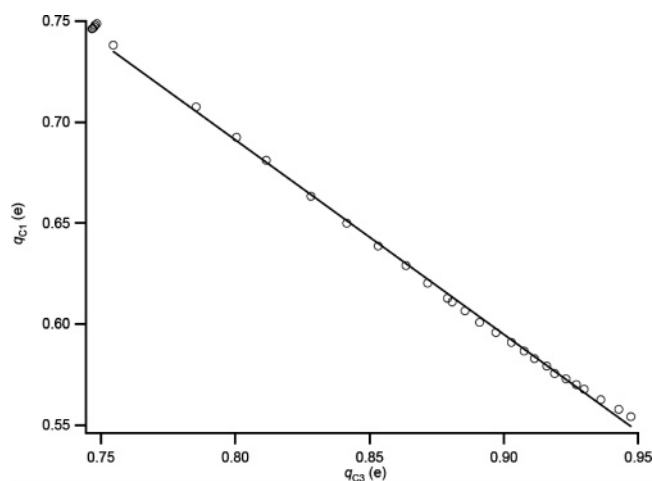

Figure 9. Plot of the integrated atomic charge on C_1 vs the integrated atomic charge on C_3 in malonaldehyde. Open symbols: Calculated points. Solid curve: Fit to a straight line with slope of -1.01.

are the Q_{zz} values for the six IHB ring atoms in malonaldehyde. As expected, the hydrogen atom has the least asymmetric charge density along the z-axis, with values of Q_{zz} close to zero, and C_2 has the most asymmetric charge density along the z-axis, with strongly negative values of Q_{zz}. Both of these quantities are relatively insensitive to variations in hydrogen-bonding distance. However, we see that C_1 and O_5, on the donor side of the molecule, experience increasing values of Q_{zz} as r decreases, indicating a less asymmetric charge distribution along the z-axis, while C_3 and O_8, on the acceptor side of the molecule, experience decreasing values of Q_{zz} as r decreases, indicating a more asymmetric charge distribution along the z-axis as r decreases. In other words, the electron density for C_1 and O_5 becomes less "π-like", and the electron density for C_3 and O_8 becomes more "π-like", as r decreases. Finally, at $r = r_{trans}$, Q_{zz} for C_1 and C_3 become equivalent, along with Q_{zz} for O_5 and O_8. Noticeably, there is no evidence of a transition occurring at the equilibrium geometry; Q_{zz} for all atoms varies smoothly over all hydrogen-bonding distances for which $r > r_{trans}$. Thus the mere redistribution of π-electron density cannot explain why
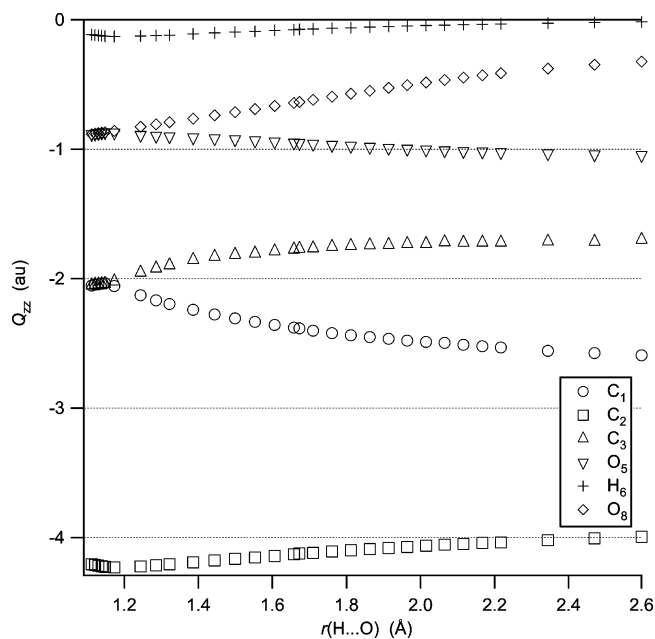

Figure 10. Plot of the zz-component of the integrated atomic quadrupole moment tensor for the six IHB ring atoms vs r.

malonaldehyde adopts the equilibrium configuration that it does, as is implied by referring to RAHB as a "feedback mechanism". Instead, the redistribution of π-electron density in the IHB ring appears to be a *reaction* to hydrogen bond formation. Indeed, since hydrogen-bond formation is inherently a σ-type interaction, the π-electron framework can really only serve as a spectator in the bond formation process. This interpretation is consistent with recent studies[95,96] on the nature of hydrogen bonding in DNA base pairs, which showed negligible π-electron transfer upon formation of A-T and G-C complexes. It is also consistent with theoretical NMR studies on malonaldehyde and its saturated analogues,[97,98] which found that the scalar coupling constants between donor and acceptor atoms were largely unaffected by the presence of a π-electron framework connecting the two; instead, the distance between donor and acceptor was primarily responsible for the magnitude of the coupling. A very recent ab initio valence bond study has also examined the effect of resonance on intermolecular hydrogen bonding.[99] In this study, the authors found that upon "switching on" the resonance effect, the hydrogen bond interaction energies were larger than if the π electrons were not permitted to delocalize. This increase in interaction energies, however, was overwhelmingly due to the electrostatic interaction between the donor and acceptor. The present findings confirm this interpretation: π electrons delocalize in malonaldehyde and its derivatives due to an inductive effect, and it is the proximity of the donor and acceptor that is chiefly responsible for the strength or weakness of the corresponding hydrogen bond. This view is also consistent with recent work on σ/π separability,[100,101] in which the σ electrons are viewed as establishing the rigid bonding framework of the molecule while the π electrons rearrange and delocalize, where appropriate, in reaction to the σ-bonding.

Conclusions

In this study, the structural, energetic, vibrational, and topological properties of the intramolecular hydrogen bond in malonaldehyde and four of its derivatives were studied by using density functional theory and a large basis set, with an aim toward examining the nonequilibrium properties of the electron density. Many of the same conclusions that have been drawn

Woodford

for intermolecular hydrogen-bonded complexes are also valid for the systems studied here, owing to the universal nature of the hydrogen bond. However, some important differences were discerned. Notably, from these calculations, it is possible to discern a transition from asymmetric to symmetric hydrogen bonding, which for these molecules occurs at a very short internuclear separation of 2.24 Å, shorter than what has been observed experimentally for neutral O−H···O intramolecular hydrogen bonds. Furthermore, the electron density at the bond critical point tends to be larger for the IHBs found in this work than for intermolecular hydrogen bonds, suggesting that the maximum threshold for $\rho_{c,HB}$ for hydrogen bonds should be revised upward. An analysis of the integrated AIM properties revealed deeper insight into the RAHB model. It was found, somewhat surprisingly, that the integrated atomic charges on the OHO hydrogen-bonding moiety remained relatively unchanged upon variation of the hydrogen bond distance; instead, significant charge transfer occurred in the π-electron framework of the carbon atoms. Future work will focus on other common intramolecular hydrogen-bonding motifs, such as derivatives of β-aminoacrolein, acetylacetone, potassium hydrogen maleate, and 9-hydroxytropolone, to derive more general relationships about intramolecular hydrogen bonding and resonance-assisted hydrogen bonding.

Supporting Information Available: Tables of selected structural properties, critical point electron density and Laplacian, differences in integrated atomic charges, energies, atomic dipole moments, and atomic volumes for the IHB hydrogen atoms, integrated atomic charge for the IHB ring atoms, and integrated *zz*-component of the atomic quadrupole moment tensor for IHB atoms. This material is available free of charge via the Internet at http://pubs.acs.org.

References and Notes

(1) Pimentel, G. C.; McClellan, A. L. *The Hydrogen Bond*; W. H. Freeman: San Francisco, CA, 1960.

(2) Kollman, P. A.; Allen, L. C. The Theory of the Hydrogen Bond. *Chem. Rev.* **1972**, *72* (3), 283−303.

(3) Jeffrey, G. A.; Saenger, W. *Hydrogen Bonding in Biological Structures*; Springer-Verlag: Berlin, Germany, 1991.

(4) Jeffrey, G. A. *An Introduction to Hydrogen Bonding*; Oxford University Press: New York, 1997.

(5) Scheiner, S. *Hydrogen Bonding: A Theoretical Perspective*; Oxford University Press: New York, 1997.

(6) Desiraju, G. R.; Steiner, T. *The Weak Hydrogen Bond*; Oxford University Press: New York, 1999.

(7) Steiner, T. The Hydrogen Bond in the Solid State. *Angew. Chem., Inte. Ed.* **2002**, *41*, 48−76.

(8) Hadzi, D. *Theoretical Treatments of Hydrogen Bonding*; John Wiley & Sons: New York, 1997.

(9) Perrin, C. L.; Nielson, J. B. "Strong" Hydrogen Bonds in Chemistry and Biology. *Annu. Rev. Phys. Chem.* **1997**, *48*, 511−544.

(10) Bader, R. F. W. *Atoms in Molecules: A Quantum Theory*, 2nd ed.; Oxford University Press: New York, 1994.

(11) Bader, R. F. W.; Essén, H. The Characterization of Atomic Interactions. *J. Chem. Phys.* **1984**, *80*, 1943−1960.

(12) Carroll, M. T.; Bader, R. F. W. An Analysis of the Hydrogen Bond in BASE-HF Complexes Using the Theory of Atoms in Molecules. *Mol. Phys.* **1988**, *65* (3), 695−722.

(13) Carroll, M. T.; Chang, C.; Bader, R. F. W. Prediction of the Structures of Hydrogen-Bonded Complexes Using the Laplacian of the Charge Density. *Mol. Phys.* **1988**, *63* (3), 387−405.

(14) Cheeseman, J. R.; Carroll, M. T.; Bader, R. F. W. The Mechanics of Hydrogen Bond Formation in Conjugated Systems. *Chem. Phys. Lett.* **1988**, *143* (5), 450−458.

(15) Koch, U.; Popelier, P. L. A. Characterization of C−H···O Hydrogen Bonds on the Basis of Charge Density. *J. Phys. Chem.* **1995**, *99*, 9747−9754.

(16) Gálvez, O.; Gómez, P. C.; Pacios, L. F. Variation with the Intermolecular Distance of Properties Dependent on the Electron Density in Hydrogen Bonding Dimers. *J. Chem. Phys.* **2001**, *115* (24), 11166−11184.

(17) Gálvez, O.; Gómez, P. C.; Pacios, L. F. Variation with the Intermolecular Distance of Properties Dependent on the Electron Density in Cyclic Dimers with Two Hydrogen Bonds. *J. Chem. Phys.* **2003**, *118* (11), 4878−4895.

(18) Pacios, L. F. Topological Descriptors of the Electron Density and the Electron Localization Function in Hydrogen Bond Dimers at Short Intermonomer Distances. *J. Phys. Chem. A* **2004**, *108*, 1177−1188.

(19) Pacios, L. F.; Gálvez, O.; Gómez, P. C. Variation of Geometries and Electron Properties along Proton Transfer in Strong Hydrogen-Bond Complexes. *J. Chem. Phys.* **2005**, *122*, 214307.

(20) Pacios, L. F. Changes with the Intermolecular Distance of Electron Properties of Hydrogen Bond Dimers at Equilibrium and Non-equilibrium Geometries. *Struct. Chem.* **2005**, *16* (3), 223−241.

(21) Espinosa, E.; Alkorta, I.; Elguero, J.; Molins, E. From Weak to Strong Interactions: A Comprehensive Analysis of the Topological and Energetic Properties of the Electron Density Distribution involving X−H···F−Y Systems. *J. Chem. Phys.* **2002**, *117* (12), 5529−5542.

(22) Buemi, G.; Zuccarello, F. Ab Initio Study of the Potential-Energy Well of Malonaldehyde on Varying the O···O Distance. *J. Chem. Soc. Faraday Trans.* **1996**, *92* (3), 347−351.

(23) Rowe, W. F.; Duerst, R. W.; Wilson, E. B. The Intramolecular Hydrogen Bond in Malonaldehyde. *J. Am. Chem. Soc.* **1976**, *98* (13), 4021−4023.

(24) Baughcum, S. L.; Duerst, R. W.; Rowe, W. F.; Smith, Z.; Wilson, E. B. Microwave Spectroscopic Study of Malonaldehyde (3-Hydroxy-2-propenal). 2. Structure Dipole Moment and Tunneling. *J. Am. Chem. Soc.* **1981**, *103*, 6296−6303.

(25) Smith, Z.; Wilson, E. B.; Duerst, R. W. The Infrared Spectrum of Gaseous Malonaldehyde (3-Hydroxy-2-propenal). *Spectrochim. Acta, Part A* **1983**, *39*, 1117−1129.

(26) Baughcum, S. L.; Smith, Z.; Wilson, E. B.; Duerst, R. W. Microwave Spectroscopic Study of Malonaldehyde. 3. Vibration−Rotation Interaction and One-Dimensional Model for Proton Tunneling. *J. Am. Chem. Soc.* **1984**, *106*, 2260−2265.

(27) Turner, P.; Baughcum, S. L.; Coy, S. L.; Smith, Z. Microwave Spectroscopic Study of Malonaldehyde. 4. Vibration−Rotation Interaction in Parent Species. *J. Am. Chem. Soc.* **1984**, *106*, 2265−2267.

(28) Firth, D. W.; Beyer, K.; Dvorak, M. A.; Reeve, S. W.; Grushow, A.; Leopold, K. R. Tunable Far-Infrared Spectroscopy of Malonaldehyde. *J. Chem. Phys.* **1991**, *94* (3), 1812−1819.

(29) Perrin, C. L.; Kim, Y. J. Symmetry of the Hydrogen Bond in Malonaldehyde Enol in Solution. *J. Am. Chem. Soc.* **1998**, *120*, 12641−12645.

(30) Baba, T.; Tanaka, T.; Morino, I.; Yamada, K. M. T.; Tanaka, K. Detection of the Tunneling-Rotation Transitions of Malonaldehyde in the Submillimeter-Wave Region. *J. Chem. Phys.* **1999**, *110*, 4131−4133.

(31) Duan, C.; Luckhaus, D. High Resolution IR-diode Laser Jet Spectroscopy of Malonaldehyde. *Chem. Phys. Lett.* **2004**, *391*, 129−133.

(32) Wassermann, T. N.; Luckhaus, D.; Coussan, S.; Suhm, M. A. Proton Tunneling Estimates for Malonaldehyde Vibrations from Supersonic Jet and Matrix Quenching Experiments. *Phys. Chem. Chem. Phys.* **2006**, *8*, 2344−2348.

(33) Frisch, M. J.; Scheiner, A. C.; Schaefer, H. F., III; Binkley, J. S. The Malonaldehyde Equilibrium Geometry: A Major Structural Shift due to the Effects of Electron Correlation. *J. Chem. Phys.* **1985**, *82* (9), 4194−4198.

(34) Luth, K.; Scheiner, S. Excited-State Energetics and Proton-Transfer Barriers in Malonaldehyde. *J. Phys. Chem.* **1994**, *98*, 3582−3587.

(35) Barone, V.; Adamo, C. Proton Transfer in the Ground and Lowest Excited States of Malonaldehyde: A Comparative Density Functional and Post-Hartree−Fock Study. *J. Chem. Phys.* **1996**, *105* (24), 11007−11019.

(36) Buemi, G.; Zuccarello, F. Importance of Steric Effect on the Hydrogen Bond Strength of Malondialdehyde and Acetylacetone 3-Substituted Derivatives. An Ab Initio Study. *Electron. J. Theor. Chem.* **1997**, *2*, 302−314.

(37) Benderskii, V. A.; Vetoshkin, E. V.; Irgibaeva, I. S.; Trommsdorff, H. P. Tunneling Splittings in Vibrational Spectra of Non-Rigid Molecules. IX. Malonaldehyde and its Isotopomers as a Test Case for Fully Coupled Multidimensional Tunneling Dynamics. *Chem. Phys.* **2000**, *262*, 393−422.

Intramolecular H Bonding in Derivatives of Malonaldehyde

J. Phys. Chem. A, Vol. 111, No. 34, 2007 **8529**

(38) Grabowski, S. J. An Estimation of Strength of Intramolecular Hydrogen Bonds—Ab Initio and AIM Studies. *J. Mol. Struct.* (*THEOCHEM*) **2001**, *562*, 137−143.

(39) Yagi, K.; Taketsugu, T.; Hirao, K. Generation of Full-Dimensional Potential Energy Surface of Intramolecular Hydrogen Atom Transfer in Malonaldehyde and Tunneling Dynamics. *J. Chem. Phys.* **2001**, *115* (23), 10647−10655.

(40) Picherri, F. Effect of Fluorine Substitution on the Proton Transfer Barrier in Malonaldehyde. A Density Functional Theory Study. *Chem. Phys. Lett.* **2003**, *376*, 781−787.

(41) Gromak, V. Ab Initio Study of Intra- and Intermolecular H-bond Energies in π-Conjugated Molecular Systems. *J. Mol. Struct.* (*THEOCHEM*) **2005**, *726*, 213−224.

(42) Shida, N.; Barbara, P. F.; Almlöf, J. E. A Theoretical Study of Multidimensional Nuclear Tunneling in Malonaldehyde. *J. Chem. Phys.* **1989**, *91* (7), 4061−4072.

(43) Latajka, Z.; Scheiner, S. Proton Transfer in the Ground and First Excited Triplet States of Malonaldehyde. *J. Phys. Chem.* **1992**, *96*, 9764−9767.

(44) Sewell, T. D.; Guo, Y.; Thompson, D. L. Semiclassical Calculations of Tunneling Splitting in Malonaldehyde. *J. Chem. Phys.* **1995**, *103* (19), 8557−8565.

(45) Sobolewski, A. L.; Domcke, W. Photophysics of Malonaldehyde: An Ab Initio Study. *J. Phys. Chem. A* **1999**, *103*, 4494−4504.

(46) Tautermann, C. S.; Voegele, A. F.; Loerting, T.; Liedl, K. R. An Accurate Semiclassical Method to Predict Ground-State Tunneling Splittings. *J. Chem. Phys.* **2002**, *117* (5), 1967−1974.

(47) Mil'nikov, G. V.; Yagi, K.; Taketsugu, T.; Nakamura, H.; Hirao, K. Tunneling Splitting in Polyatomic Molecules: Application to Malonaldehyde. *J. Chem. Phys.* **2003**, *119* (1), 10−13.

(48) Coutino-Neto, M. D.; Viel, A.; Manthe, U. The Ground State Tunneling Splitting of Malonaldehyde: Accurate Full Dimensional Quantum Dynamics Calculations. *J. Chem. Phys.* **2004**, *121* (19), 9207−9210.

(49) Coe, J. D.; Martínez, T. J. Ab Initio Molecular Dynamics of Excited-State Intramolecular Proton Transfer around a Three State Conical Intersection in Malonaldehyde. *J. Phys. Chem. A* **2006**, *110*, 618−620.

(50) Sirois, S.; Proynov, E. I.; Nguyen, D. T.; Salahub, D. R. Hydrogen-Bonding in Glycine and Malonaldehyde: Performance of the Lap1 Correlation Functional. *J. Chem. Phys.* **1997**, *107* (17), 6770−6781.

(51) Bader, R. F. W. Pauli Repulsions Exist Only in the Eye of the Beholder. *Chem. Eur. J.* **2006**, *12*, 2896−2901.

(52) Poater, J.; Solà, M.; Bickelhaupt, F. M. A Model of the Chemical Bond Must Be Rooted in Quantum Mechanics, Provide Insight, and Possess Predictive Power. *Chemistry: A European Journal* **2006**, *12*, 2902−2905.

(53) Matta, C. F.; Hernandez-Trujillo, J.; Tang, T. H.; Bader, R. F. W. Hydrogen−Hydrogen Bonding: A Stabilizing Interaction in Molecules and Crystals. *Chem. Eur. J.* **2003**, *9*, 1940−1951.

(54) Haaland, A.; Shorokhov, D. J.; Tverdova, N. V. Topological Analysis of Electron Densities: Is the Presence of an Atomic Interaction Line in an Equilibrium Geometry a Sufficient Condition for the Existence of a Chemical Bond? *Chem. Eur. J.* **2004**, 10, 4416−4421.

(55) Grabowski, S. J. Hydrogen Bonding Strength—Measures Based on Geometric and Topological Parameters. *J. Phys. Org. Chem.* **2004**, *17*, 18−31.

(56) Gilli, G.; Bellucci, F.; Ferretti, V.; Bertolasi, V. Evidence for Resonance-Assisted Hydrogen Bonding from Crystal-Structure Correlations on the Enol Form of the β-Diketone Fragment. *J. Am. Chem. Soc.* **1989**, *111*, 1023−1028.

(57) Gilli, G.; Gilli, P. Towards a Unified Hydrogen-Bond Theory. *J. Mol. Struct.* **2000**, *552*, 1−15.

(58) Garcia-Viloca, M.; González-Lafont, A.; Lluch, J. M. On pK_a Matching as a Requirement to Form a Low-Barrier Hydrogen Bond. A Theoretical Study in Gas Phase. *J. Phys. Chem. A* **1997**, *101*, 3880−3886.

(59) Becke, A. D. Density-Functional Thermochemistry. III. The Role of Exact Exchange. *J. Chem. Phys.* **1993**, *98* (7), 5648−5652.

(60) Stephens, P. J.; Devlin, F. J.; Chabalowski, C. F.; Frisch, M. J. Ab Initio Calculation of Vibrational Absorption and Circular Dichroism Spectra using Density Functional Force Fields. *J. Phys. Chem.* **1994**, *98* (45), 11623−11627.

(61) Hertwig, R. H.; Koch, W. On the Parameterization of the Local Correlation Functional. What Is Becke-3-LYP? *Chem. Phys. Lett.* **1997**, *268*, 345−351.

(62) Schmidt, M. W.; Baldridge, K. K.; Boatz, J. A.; Elbert, S. T.; Gordon, M. S.; Jensen, J. H.; Koseki, S.; Matsunaga, N.; Nguyen, K. A.; Su, S. J.; Windus, T. L.; Dupuis, M.; Montgomery, J. A. General Atomic and Molecular Electronic Structure System. *J. Comput. Chem.* **1993**, *14*, 1347−1363.

(63) Biegler-König, F. W.; Bader, R. F. W.; Tang, T. H. Calculation of the Average Properties of Atoms in Molecules. II. *J. Comput. Chem.* **1982**, *3*, 317−328.

(64) Mohajeri, A. Theoretical Evidences for Resonance-Assisted Hydrogen Bonding. *J. Mol. Struct.* (*THEOCHEM*) **2004**, *678*, 201−205.

(65) The authors of the original paper assumed an OH bond length of 0.969 Å.

(66) Nishimura, Y.; Ujita, H.; Sekiya, H. Structures and Proton Transfer of Malonaldehyde and its Chloroderivatives. *Kyushu Daigaku Sogorikogaku Kenkyuka Hokoku* **1993**, *15*, 187−194.

(67) Tayyari, S. F.; Moosavi-Tekyeh, Z.; Zahedi-Tabrizi, M.; Eshghi, H.; Emampour, J. S.; Rahemi, H.; Hassanpour, M. Intramolecular Hydrogen Bonding in 2-Nitromalonaldehyde: Infrared Spectrum and Quantum Chemical Calculations. *J. Mol. Struct.* **2006**, *782*, 191−199.

(68) Buemi, G.; Zuccarello, F. DFT Study of the Intramolecular Hydrogen Bonds in the Amino and Nitro Derivatives of Malonaldehyde. *Chem. Phys.* **2004**, *306*, 115−129.

(69) Tayyari, S. F.; Milani-Nejad, F. On the Reassignment of Vibrational Frequencies of Malonaldehyde. *Spectrochim. Acta A* **1998**, *54*, 255−263.

(70) Bellamy, L. J.; Pace, R. J. The Significance of Infra-red Frequency Shifts in Relation to Hydrogen Bond Strengths. *Spectrochim. Acta A* **1969**, *25*, 319−328.

(71) Bellamy, L. J.; Owen, A. J. A Simple Relationship between the Infra-red Stretching Frequencies and the Hydrogen Bond Distance in Crystals. *Spectrochim. Acta A* **1969**, *25*, 329−333.

(72) Rozas, I.; Alkorta, I.; Elguero, J. Intramolecular Hydrogen Bonds in *ortho*-Substituted Hydroxybenzenes and in 8-Substituted 1-Hydroxynaphthalenes: Can a Methyl Group Be an Acceptor of Hydrogen Bonds? *J. Phys. Chem. A* **2001**, *105*, 10462−10467.

(73) Espinosa, E.; Molins, E. Retrieving Interaction Potentials from the Topology of the Electron Density Distribution: The Case of Hydrogen Bonds. *J. Chem. Phys.* **2000**, *113* (14), 5686−5694.

(74) Jablonski, M.; Kaczmarek, A.; Sadlej, A. J. Estimates of the Energy of Intramolecular Hydrogen Bonds. *J. Phys. Chem. A* **2006**, *110*, 10890−10898.

(75) Musin, R. N.; Mariam, Y. H. An Integrated Approach to the Study of Intramolecular Hydrogen Bonds in Malonaldehyde Enol Derivatives and Naphthazarin: Trend in Energetic versus Geometrical Consequences. *J. Phys. Org. Chem.* **2006**, *19*, 425−444.

(76) Ichikawa, M. The O−H vs O···O Distance Correlation, the Geometric Isotope Effect in OHO Bonds, and Its Application to Symmetric Bonds. *Acta Crystallogr.*, *Sect. B* **1978**, *34*, 2074−2080.

(77) Steiner, T.; Saenger, W. Lengthening of the Covalent O−H Bond in O−H···O Hydrogen Bonds Re-examined from Low-Temperature Neutron Diffraction Data of Organic Compounds. *Acta Crystallogr.*, *Sect. B* **1994**, *50*, 348−357.

(78) Korth, H. G.; de Heer, M. I.; Mulder, P. A DFT Study on Intramolecular Hydrogen Bonding in 2-Substituted Phenols: Conformations Enthalpies and Corrections with Solute Parameters. *J. Phys. Chem. A* **2002**, *106*, 8779−8789.

(79) Abraham, M. H.; Grellier, P. L.; Prior, D. V.; Taft, R. W.; Morris, J. J.; Taylor, P. J.; Laurence, C.; Berthelot, M.; Doherty, R. M.; Kamlet, M. J.; Abbout, J. L. M.; Sraidi, K.; Guihéneuf, G. A General Treatment of Hydrogen Bond Complexation Constants in Tetrachloromethane. *J. Am. Chem. Soc.* **1988**, *110*, 8534−8536.

(80) Grabowski, S. J.; Dubis, A. T.; Martynowski, D.; Główka, M.; Palusiak, M.; Leszczynski, J. Crystal and Molecular Structure of Pyrrole-2-carboxylic Acid: π-Electron Delocalization of Its Dimers—DFT and MP2 Calculations. *J. Phys. Chem. A* **2004**, *108*, 5815−5822.

(81) Domagala, M.; Grabowski, S. J. C−H···N and C−H···S Hydrogen Bonds—Influence of Hybridization on Their Strength. *J. Phys. Chem. A* **2005**, *109*, 5683−5688.

(82) Jenkins, S.; Morrison, I. The Chemical Character of the Intermolecular Bonds of Seven Phases of Ice as Revealed by Ab Initio Calculation of Electron Densities. *Chem. Phys. Lett.* **2000**, *317*, 97−102.

(83) Flaig, R.; Koritsanszky, T.; Dittrich, B.; Wagner, A.; Luger, P. Intra- and Intermolecular Topological Properties of Amino Acids: A Comparative Study of Experimental and Theoretical Results. *J. Am. Chem. Soc.* **2002**, *124*, 3407−3417.

(84) Mallinson, P. R.; Smith, G. T.; Wilson, C. C.; Grech, E.; Wozniak, K. From Weak Interactions to Covalent Bonds: A Continuum in the Complexes of 1,8-Bis(dimethylamino)naphthalene. *J. Am. Chem. Soc.* **2003**, *125*, 4259−4270.

(85) Tang, T. H.; Deretey, E.; Jensen, S. J. K.; Csizmadia, I. G. Hydrogen Bonds: Relation Between Lengths and Electron Densities at Bond Critical Points. *Eur. Phys. J. D* **2006**, *37*, 217−222.

(86) Gibbs, G. V.; Cox, D. F.; Crawford, T. D.; Rosso, K. M.; Ross, N. L.; Downs, R. T. Classification of Metal-Oxide Bonded Interactions Based on Local Potential- and Kinetic-Energy Densities. *J. Chem. Phys.* **2006**, *124*, 084704.

(87) Espinosa, E.; Souhassou, M.; Lachekar, H.; Lecomte, C. Topological Analysis of the Electron Density in Hydrogen Bonds. *Acta Crystallogr.*, *Sect. B* **1999**, *55*, 563−572.

(88) Knop, O.; Rankin, K. N.; Boyd, R. J. Coming to Grips with N−H···N Bonds. 1. Distance Relationships and Electron Density at the Bond Critical Point. *J. Phys. Chem. A* **2001**, *105*, 6552−6566.

Woodford

(89) Chěcińska, L.; Grabowski, S. J. Partial Hydrogen Bonds: Structural Studies on Thioureidoalkylphosphonates. *J. Phys. Chem. A* **2005**, *109*, 2942−2947.

(90) Alkorta, I.; Rozas, I.; Elguero, J. The Additive Properties of the Electron Density at the Bond Critical Points in Hydrogen-Bonded Complexes. *J. Mol. Struct.* (*THEOCHEM*) **1998**, *452*, 227−232.

(91) Grabowski, S. J. Ab Initio Calculations on Conventional and Unconventional Hydrogen Bonds−Study of the Hydrogen Bond Strength. *J. Phys. Chem. A* **2001**, *105*, 10739−10746.

(92) Guerra, C. F.; Handgraaf, J.-W.; Baerends, E. J.; Bickelhaupt, F. M. Voronoi Deformation Density (VDD) Charges: Assessment of the Mulliken Bader Hirshfeld Weinhold and VDD Methods for Charge Analysis. *J. Comput. Chem.* **2004**, *25*, 189−210.

(93) Mandado, M.; Van Alsenoy, C.; Mosquera, R. Joint QTAIM and Hirshfeld Study of the σ and π Charge Distribution and Electron Delocalization in Carbonyl Compounds: A Comparative Study with the Resonance Model. *J. Phys. Chem. A* **2005**, *109*, 8624−8631.

(94) Madsen, G. K. H.; Iversen, B. B.; Larsen, F. K.; Kapon, M.; Reisner, G. M.; Herbstein, F. H. Topological Analysis of the Charge Density in Short Intramolecular O−H···O Hydrogen Bonds. Very Low Temperature X-ray and Neutron Diffraction Study of Benzoylacetone. *J. Am. Chem. Soc.* **1998**, *120*, 10040−10045.

(95) Guerra, C. F.; Bickelhaupt, F. M.; Snijders, J. G.; Baerends, E. J. The Nature of the Hydrogen Bond in DNA Base Pairs: The Role of Charge Transfer and Resonance Assistance. *Chem. Eur. J.* **1999**, *5*, 3581−3594.

(96) Guerra, C. F.; Bickelhaupt, F. M. Orbital Interactions and Charge Redistribution in Weak Hydrogen Bonds: The Watson−Crick AT Mimic Adenine-2,4-difluorotoluene. *J. Chem. Phys.* **2003**, *119*, 4262−4273.

(97) Alkorta, I.; Elguero, J.; Mó, O.; Yáñez, M.; Del Bene, J. E. Do Coupling Constants and Chemical Shifts Provide Evidence for the Existence of Resonance-Assisted Hydrogen Bonds? *Mol. Phys.* **2004**, *102* (23−24), 2563−2574.

(98) Alkorta, I.; Elguero, J.; Mó, O.; Yáñez, M.; Del, Bene, J. E. Are Resonance-Assisted Hydrogen Bonds 'Resonance Assisted'? A Theoretical NMR Study. *Chem. Phys. Lett.* **2005**, *411*, 411−415.

(99) Beck, J. F.; Mo, Y. How Resonance Assists Hydrogen Bonding Interactions: An Energy Decomposition Analysis. *J. Comput. Chem.* **2007**, *28*, 455−466.

(100) Shaik, S. S.; Hiberty, P. C.; Lefour, J. M.; Ohanessian, G. Is Delocalization a Driving Force in Chemistry? Benzene, Allyl Radical, Cyclobutadiene, and their Isoelectronic Species. *J. Am. Chem. Soc.* **1987**, *109* (2), 363−374.

(101) Shaik, S. S.; Shurki, A.; Danovich, D.; Hiberty, P. C. A Different Story of π-Delocalization−The Distortivity of π-Electrons and Its Chemical Manifestations. *Chem. Rev.* **2001**, *101* (1501−1539), 1501.